An Investigation on the Property and Fast Implementation of a Ray-driven Method for Inversion of the Attenuated Radon Transform with Variable Focusing Fan-beam Collimators

Junhai Wen, Zigang Wang, Bin Li, and Zhengrong Liang, *Member, IEEE*

***Abstract* -- Single photon emission computed tomography (SPECT) is based on the measurement of radiation emitted by a radiotracer injected into the patient. Because of photoelectric absorption and Compton scatter, the gamma photons are attenuated inside the body before arriving at the detector. A quantitative reconstruction must consider the attenuation, which is usually non-uniform. Novikov had derived an explicit inversion formula for the non-uniformly attenuated Radon transform for SPECT reconstruction of parallel-beam collimated projections. In our previous work, we extended his work to variable focusing fan-beam (VFF) collimators. A ray-driven analytical inversion formula for VFF reconstruction with non-uniform attenuation was derived. The drawback of ray-driven based reconstruction is time consuming. In this work, we proposed a fast implementation method. Based on the property of ray-driven strategy, we calculated the reconstruction contribution of every ray for every reconstruction point in advance and saved them into database. When performing the reconstruction, we loaded the saved database, multiplied it by the corresponding rays and added the contributions of all rays together. The final image is then obtained efficiently by computing a divergence equation from the contributions. In addition to the software optimization, we utilized the texture mapping architecture of PC graphics/video card to accelerate the speed of the image reconstruction. We further investigated the property of the associated artifacts in the analytical inversion of the attenuated Radon transform. The artifacts were remarkably reduced when more projections were sampled to mitigate the problem of wide bandwidth of discrete Hilbert transform.**

I. Introduction

In single-photon emission computed tomography (SPECT), because of photoelectric absorption and Compton scatter, the gamma photons are attenuated inside the body before arriving at the detector. Quantitative reconstruction of the radiotracer uptake concentration at any location inside the body requires accurate compensation for the attenuation, which is usually non-uniform. Mathematically the reconstruction task can be formulated as an inversion of the attenuated Radon transform. A great research interest on analytical inversion of the attenuated Radon transform for quantitative SPECT image reconstruction with non-uniform attenuation and parallel-beam geometry has been seen in the last decade. Arbuzov, *et al.* [1] presented an inversion of the attenuated Radon transform with non-uniform attenuation, but their result was not cast in the well-established filtered backprojection (FBP) form, which was later derived by Novikov [2]. In Novikov's work, an explicit inversion formula for the non-uniformly attenuated Radon transform for parallel-beam geometry was derived. This formula had been implemented and good reconstruction results were obtained [3]. Another version of the explicit inversion formula was later reported by Natterer [4], also for a parallel-beam geometry.

For many clinical applications, however, fan-beam and variable focusing fan-beam (VFF) collimation geometries are preferred. Fan-beam collimator improves count density and spatial resolution, as compared to parallel-hole collimator, for imaging small objects, such as animals and the human head and breasts. For cardiac studies, however, the fan-beam geometry encounters truncation problem, due to its limited acceptance angle across the field-of-view (FOV), which can cause artifacts. Variable focusing fan-beam collimator overcomes this truncation problem, while preserving the improved count density and spatial resolution.

In our previous work, we proposed an approximate reconstruction algorithm with non-uniform attenuation for fan-beam and VFF collimators and obtained very good reconstruction results [5]. An exact ray-driven analytical formula for VFF reconstruction with non-uniform attenuation was obtained in [6]. But the drawback of ray-driven based reconstruction is time consuming. In this work, we proposed a

Manuscript submitted on October 20, 2003. This work was supported in part by NIH National Heart, Lung and Blood Institute under Grant No. HL54166.

J. Wen is with the Department of Radiology, State University of New York, Stony Brook, NY 11794, USA (telephone: 631-444-7999, e-mail: wenjh@mil.sunysb.edu).

Z. Wang and Bin Li are with the Department of Radiology, State University of New York, Stony Brook, NY 11794, USA.

Z. Liang is with the Departments of Radiology and Computer Science, State University of New York, Stony Brook, NY 11794, USA.

fast implementation method. Based on the property of ray-driven strategy, we calculated the reconstruction contribution of every ray for every reconstruction point in advance and saved them into a database or disk space. When performing the reconstruction, the database was loaded. The image was then reconstructed efficiently from these contributions. In addition to the algorithm optimization, the texture mapping architecture of the PC graphics/video card was utilized to accelerate the reconstruction speed. We further investigated the property of the associated artifacts in the analytical inversion of the attenuated Radon transform.

II. The Ray-driven Method for Inversion of the Non-uniformly Attenuated Radon Transform with Variable Focusing Fan-beam Collimators

In SPECT imaging, the measured projection data at angle ϕ can be expressed as

$$g_\phi(x_r) = \int_{-\infty}^{\infty} \exp[-(D_\phi a_\phi)(x_r, y_r)] f_\phi(x_r, y_r) dy_r \qquad (1)$$

where $f(x,y)$ denotes the activity source distribution to be reconstructed and $a(x,y)$ is the non-uniform attenuation coefficient map across the body. Note that $g_\phi(x_r)$ is the projection datum at position x_r with projection angle ϕ. The relation between the stationary coordinates (x,y) and the rotated coordinates (x_r, y_r) is

$$\begin{aligned} x_r &= x\cos\phi + y\sin\phi \\ y_r &= -x\sin\phi + y\cos\phi \end{aligned}.$$

The divergent beam transform is

$$\begin{aligned} (D_\phi a_\phi)(x_r, y_r) &= D_\phi\{a_\phi(x_r, y_r)\} \\ &= \int_{y_r}^{\det ector} a_\phi(x_r, y_r')\, dy_r' . \end{aligned} \qquad (2)$$

In SPECT, the gamma photons are attenuated before arriving at the detector, so $\exp[-(D_\phi a_\phi)(x_r, y_r)]$ is the attenuation of gamma photons emitted from point (x_r, y_r) before they arrive at the detector with angle of ϕ.

We know that any ray (p,β) in the VFF geometry can be seen as a ray (x_r,ϕ) in parallel-beam geometry (see Fig. 1 below). Let $D(p)$ be the variable focal length. The relation between the parallel-hole and VFF geometries is

$$\begin{aligned} \phi &= \beta + \gamma = \beta + \arctan\frac{p}{D(p)} \\ x_r &= p\cos\gamma = \frac{pD(p)}{\sqrt{D(p)^2 + p^2}} \end{aligned}. \qquad (3)$$

For each ray (p,β), we can build a local coordinate system (u,v). The relation between this local coordinate system and the original coordinate system is

$$\begin{aligned} u &= x\cos\phi + y\sin\phi \\ v &= -x\sin\phi + y\cos\phi \end{aligned}. \qquad (4)$$

In this local coordinate system, ray (p,β) will be a parallel-beam ray. So we can use our parallel-beam ray-driven reconstruction formula to calculate the reconstruction contribution of this ray for every reconstruction points in the image domain. For any point (x,y), its position in this local coordinate system is (u,v).

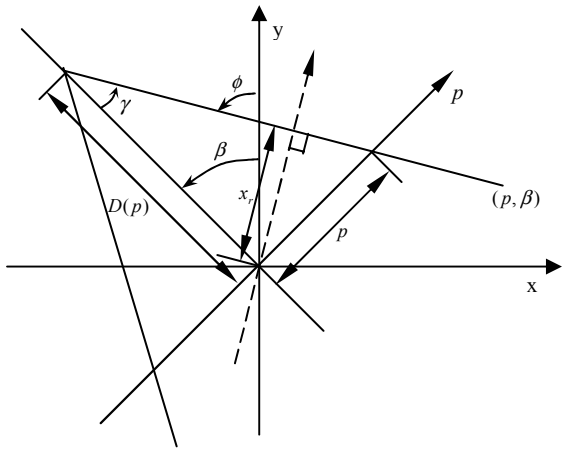

Fig. 1: The relation between parallel-beam and VFF geometry.

In [6], our ray-driven analytical VFF reconstruction formula was obtained as

$$f(x,y) = \frac{1}{4\pi}\left(\frac{\partial}{\partial x}B_C(x,y) + \frac{\partial}{\partial y}B_S(x,y)\right) \qquad (5)$$

$$\begin{aligned} B_C(x,y) &= \int_0^{2\pi}\int_{-\infty}^{\infty}[e^{(D_\phi a_\phi)(u,v)} g a_{(\beta,p)}(u)]\cos\phi\,|J|\,dp d\beta \\ B_S(x,y) &= \int_0^{2\pi}\int_{-\infty}^{\infty}[e^{(D_\phi a_\phi)(u,v)} g a_{(\beta,p)}(u)]\sin\phi\,|J|\,dp d\beta \end{aligned} \qquad (6)$$

where the Jacobian $|J|$ is given by

$$|J| = \begin{vmatrix} \partial x_r/\partial p & \partial x_r/\partial\beta \\ \partial\phi/\partial p & \partial\phi/\partial\beta \end{vmatrix} = \frac{D^3(p) + p^3 D'(p)}{\sqrt{(D^2(p) + p^2)^3}}$$

and

$$\begin{aligned} & g a_{(\beta,p)}(u) \\ &= e^{-A_\phi(u)}[\cos(E_\phi(u))H\{\cos(E_\phi(x_r))e^{A_\phi(x_r)} g(p,\beta)\delta(u - x_r)\} \\ &+ \sin(E_\phi(u))H\{\sin(E_\phi(x_r))e^{A_\phi(x_r)} g(p,\beta)\delta(u - x_r)\}] \end{aligned}$$

$$E_\phi(u) = H\{A_\phi(u)\}, \text{ and } A_\phi(u) = \frac{1}{2} R_\phi\{a_\phi(u,v)\}. \quad (7)$$

where R represents the Radon transform and H denotes the Hilbert transform. The relation between (x,y) and (u,v) is shown by equation (4). The relation between (p,β) and (x_r,ϕ) is shown by equation (3). Therefore, (u,v) can be determined by (x,y), and (x_r,ϕ) can be obtained by (p,β).

For each ray in the local coordinate system, this ray is a parallel-beam ray, and the position of this ray is at (x_r,ϕ). Using equation (6) and equation (7), the reconstruction contributions of this ray to every reconstruction points across FOV is calculated first and then back-projected to these reconstruction points with different weights according to the equations. By a ray-by-ray manner, after all VFF rays are calculated, two images $B_c(x,y)$ and $B_s(x,y)$ are obtained, *i.e.*, $(B_c(x,y), B_s(x,y))$ being a vector image. By using equation (5), we can compute the reconstructed image.

III. Fast Implementation Method of the Ray-driven Reconstruction with Non-uniform Attenuation

Our algorithm is based on a ray-driven strategy. The problem of ray-driven based reconstruction is time consuming. In this work, we proposed a fast implementation method. Based on the property of ray-driven strategy above, we calculate the reconstruction contributions of every ray for every reconstruction points in advance (see Fig. 2), and save

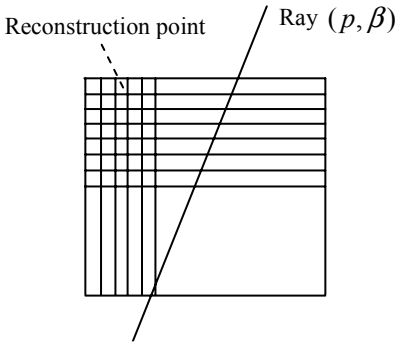

Fig. 2: Reconstruction point and ray.

them into a database or disk space. If the size of the reconstructed image is KxK, the number of projections is M and the bins of each projection is N, we need MxN contribution images to be saved in the database. When performing the reconstruction, we only need to load the database and multiply it by the corresponding rays, and then add the contribution images of all rays together with different weights of $\cos\phi$ or $\sin\phi$. The results are $B_C(x,y)$ and $B_S(x,y)$ (see Fig. 3). The final image is reconstructed by using equation (5).

For ray (p,β), its reconstruction contribution image is

$$C_{(\beta,p)}(x,y) = [e^{(D_\phi a_\phi)(u,v)} g a_{(\beta,p)}(u)]|J| \quad (8)$$

where

$$\begin{aligned} & g a_{(\beta,p)}(u) \\ &= e^{-A_\phi(u)}[\cos(E_\phi(u)) H\{\cos(E_\phi(x_r)) e^{A_\phi(x_r)} \delta(u-x_r)\} \\ &+ \sin(E_\phi(u)) H\{\sin(E_\phi(x_r)) e^{A_\phi(x_r)} \delta(u-x_r)\}] \end{aligned}$$

$$E_\phi(u) = H\{A_\phi(u)\}, \text{ and } A_\phi(u) = \frac{1}{2} R_\phi\{a_\phi(u,v)\}.$$

If the number of projections is M and the number of bins of each projection is N, we have MxN contribution images:

$$C_{(\beta_i,p_j)}(x,y), i = 0,1,...,M-1; j = 0,1,...,N-1.$$

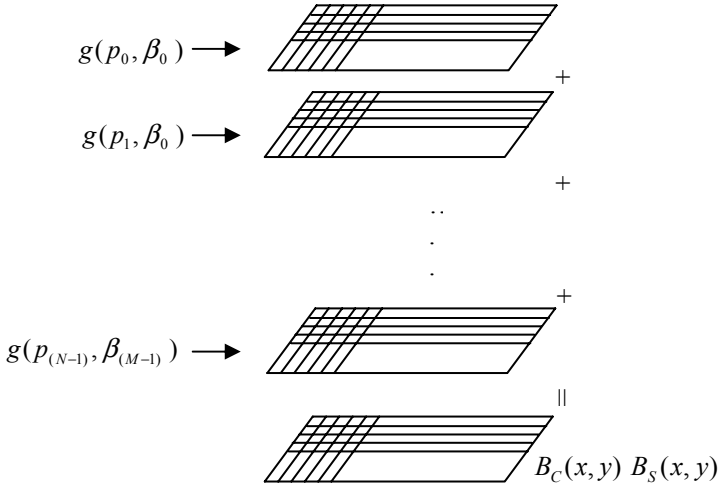

Fig. 3: Fast reconstruction of ray-driven algorithm.

When performing the reconstruction, we only need to load the these contribution images, the reconstruction is given by

$$f(x,y) = \frac{1}{4\pi}\left(\frac{\partial}{\partial x} B_C(x,y) + \frac{\partial}{\partial y} B_S(x,y)\right) \quad (9)$$

$$B_C(x,y) = \sum_{i=0}^{M-1}\sum_{j=0}^{N-1} g(\beta_i, p_j) C_{(\beta_i,p_j)}(x,y)\cos\phi_{i,j}$$

$$B_S(x,y) = \sum_{i=0}^{M-1}\sum_{j=0}^{N-1} g(\beta_i, p_j) C_{(\beta_i,p_j)}(x,y)\sin\phi_{i,j} \quad (10)$$

where

$$\phi_{i,j} = \beta_i + \arctan\frac{p_j}{D(p_j)}. \quad (11)$$

and $g(\beta_i, p_j)$ is projection.

IV. Accelerating Image Reconstruction by Hardware Technologies

Due to the large amount of the rotation and interpolation operations in our ray-driven reconstruction algorithm, the computation is intensive for the currently available CPU and RAM capacities. Due to the game marketing drive force, the PC video card has been developed to handle a large dataset in real time manner. Its 2D/3D texture mapping architecture is readily available to speedup the operations. We implemented our reconstruction algorithm by Windows 2000 operating system on a PC platform of Pentium 4 with a CPU speed of 1.7 GHz and memory of 1GB RAM and a Nvidia@ Gforce3 graphics board of 64 MB RAM.

The implementation of the image reconstruction operations is similar to that of accelerating rendering of 3D image datasets. A modern graphics card provides a flexible and programmable hardware means to implement the 3D transverse and texture processing for image rendering. For example, the Nvidia@ Gforce3 graphics card supports multi-texture and "texture shader" technologies for the programmable texture processing. Using these technologies, we can accelerate our reconstruction algorithm in two stages:

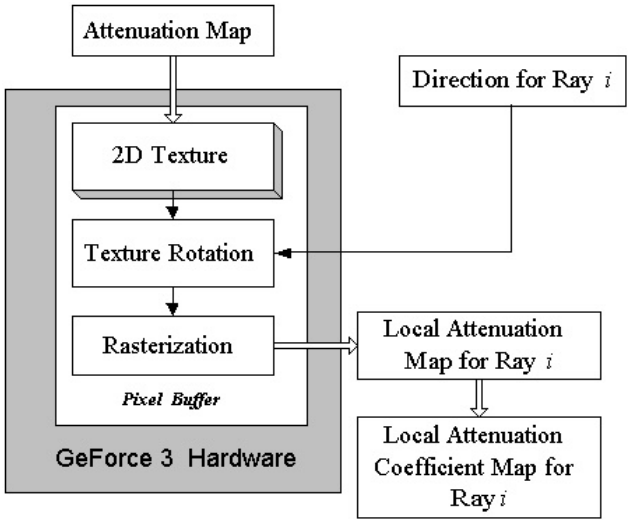

Fig. 4: The flowchart of hardware acceleration on the rotation and re-sampling of the attenuation map.

A. Rotation of the attenuation map

In our ray-driven reconstruction algorithm, the attenuation map needs to be rotated and re-sampled for each ray. These two operations are time consuming. At this first stage, the rotation and re-sampling of the attenuation map were implemented by traditional graphics pipeline with hardware acceleration (see Fig. 4).

B. Back-projection operation

For each ray, the local attenuation coefficient map generated by the first stage and the corresponding weighted map are needed to be rotated to its original angle for implementation of equation (8). The multi-texture operations, such as addition and multiply, were utilized for this task (see Fig. 5). Because there are several exponent operations in equation (8), it is not easy to implement the whole procedure using the hardware operation only. We then employed the fast CPU speed to perform other exponent operations.

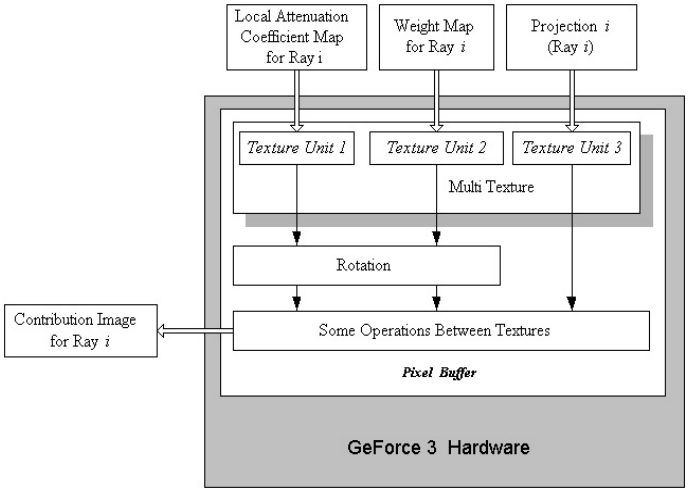

Fig. 5: The flowchart of hardware acceleration in the back-projection.

After using the PC video card hardware acceleration, the whole reconstruction time is reduced from original 30 minutes to about 3 minutes, which includes the time for calculating the contribution images of all rays and the time for performing the final image reconstruction. Further investigations are under progress for more efficiently use of the hardware. More than 10 folds reduction of computing time is expected.

V. The Property of the Artifacts in the Ray-driven Reconstruction with Non-uniform Attenuation

In the ray-driven non-uniform attenuation reconstruction, the projection along each ray is a point. This requires that the involved discrete Hilbert transform has a wide bandwidth. But this wide bandwidth requirement usually does not provide a smooth property in the spatial domain. This causes some artifacts in the reconstructed images. In this work, we investigated the property of these artifacts, and found that if more projections were acquired, the artifacts in the reconstructed images could be remarkably reduced (see Fig. 6). In Figure 6, picture (a) is the activity phantom. Picture (b) is the attenuation map. Pictures (c) and (d) are the reconstructed images from VFF projections of 128 views each with 128 bins and of 256 views each with 128 bins, respectively. The focal length is $D(p)=300+30|p|$. It is observed that when more projections were acquired, less artifacts in the reconstructed images were seen. Pictures (e) and (f) are the reconstructed images from fan-beam projections of 128 views each with 128 bins and of 256 views each with 128 bins, respectively. The focal length is D=300. The same trend of generating the artifacts was seen in both fan-bean and VFF reconstruction results. This observation concurs with that in the parallel-hole reconstruction results [2, 3], indicating that the discrete Hilbert transform needs special attention in implementation.

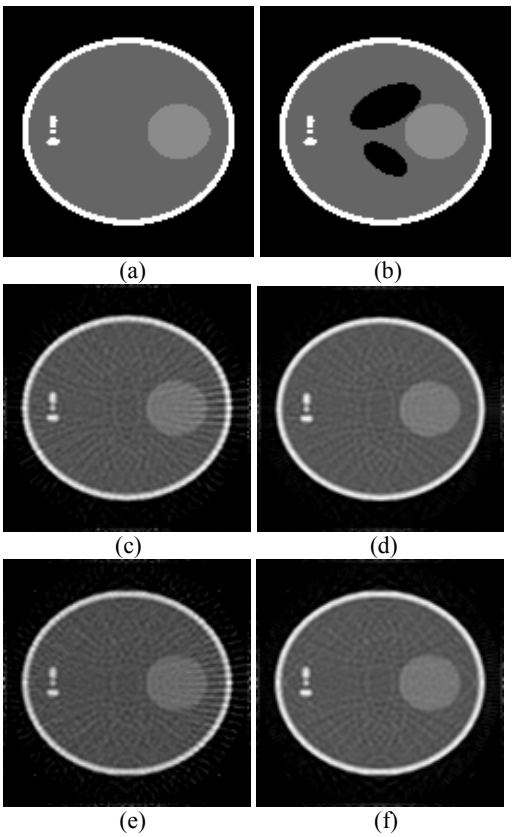

Fig. 6: Reconstruction results with different number of projections. (a) is the activity phantom. (b) is attenuation map. (c) is the reconstructed image from VFF projections of 128 views each with 128 bins. (d) is the reconstructed image from VFF projections of 256 views each with 128 bins. The focal length is $D(p)=300+30|p|$. (e) is the reconstructed image from fan-beam projections of 128 views each with 128 bins. (f) is the reconstructed image from fan-beam projections of 256 views each with 128 bins. The focal length is D=300.

VI. Conclusions

In this work, we proposed a fast implementation method. Based on the property of ray-driven strategy, we calculated the reconstruction contributions of each ray for all associated reconstruction points across the FOV in advance and saved them into a database or disk space. When performing the reconstruction, we loaded the database, multiplied it by the corresponding rays and added the contributions of all rays together. The final image is then computed efficiently by a divergence equation from these contributions. In addition to the algorithm optimization on fast CPU and memory, we explored the capability of PC graphics/video card to accelerate the reconstruction speed. More than ten fold reduction of computing time was observed by the use of the hardware.

We also investigated the property of the associated artifacts in the reconstruction. These artifacts were remarkably reduced when more projections were sampled to mitigate the problem of wide bandwidth of the discrete Hilbert transform. Further investigations on the properties of the artifacts are currently under progress.

VII. References

[1] E.V. Arbuzov, A.L. Bukhgeim,. and S.G. Kazantsev, "Two-dimensional tomography problems and the theory of A-analytic functions", *Siberian Advances in Mathematics*, vol. 8, no. 4, pp. 1-20, 1998.

[2] R. Novikov, "An inversion formula for the attenuated X-ray transformation", Preprint, May 2000.

[3] L. Kunyansky, "A new SPECT reconstruction algorithm based on the Novikov's explicit inversion formula", *Inverse Problems*, vol. 17, pp. 293-306, 2001.

[4] F. Natterer, "Inversion of the attenuated Radon transform", *Inverse Problems*, vol. 17, pp. 113-119, 2001.

[5] J. Wen, T. Li, X. Li, and Z. Liang, "Fan-beam and variable-focal-length fan-beam SPECT reconstruction with non-uniform attenuation", *J. Nucl. Medicine Technology*, vol. 30, pp. 97, 2002.

[6] J. Wen, T. Li and Z. Liang, "An analytical inversion of non-uniformly attenuated Radon transform with variable focal-length fan-beam collimators", *IEEE Trans. Nuclear Sci*ence, vol. 50, no. 5, pp. 1541-1549, 2003.

[7] L. Shepp and B. Logan, "The Fourier reconstruction of a head section", *IEEE Trans. Nuclear Science*, vol. 21, pp. 21-43, 1974.

[8] Gabort Herman, *Image Reconstruction from Projections*, ACADEMIC PRESS, INC. New York, USA, 1980.

[9] G. T. Gullberg, *The Attenuated Radon Transform: Theory and application in medicine and biology*, Ph.D. Dissertation, University of California at Berkeley, CA, 1979.

[10] J. You, Z. Liang, and G. L. Zeng, "A unified reconstruction framework for both parallel-beam and variable focal-length fan-beam collimators by a Cormack-type inversion of exponential Radon transform", *IEEE Trans. Medical Imaging*, vol. 18, pp. 59-65, 1999.

[11] J. Wen, T. Li, and Z. Liang, "Ray-driven analytical fan-beam SPECT reconstruction with non-uniform attenuation", *Proc. IEEE Intl. Sym. on Biomedical Imaging*, pp. 629-632, 2002.